



ELSEVIER

Available online at www.sciencedirect.com

SCIENCE @ DIRECT®

Optics Communications 214 (2002) 39–45

OPTICS
COMMUNICATIONS

www.elsevier.com/locate/optcom

Large dielectric non-spherical particle in an evanescent wave field near a plane surface

Yuri Eremin^a, Thomas Wriedt^{b,*}

^a Department of Applied Mathematics and Computer Science, Moscow State University, Vorobyov Hills, Moscow 119899, Russia

^b Institut für Werkstofftechnik, Badgasteiner Str. 3, 28359 Bremen, Germany

Received 12 April 2002; received in revised form 28 June 2002; accepted 28 October 2002

Abstract

In this paper we present an extended scheme of the Discrete Sources Method applied to the analysis of scattering of evanescent waves by a large particle deposited on a prism surface. Computer simulation results relating to the influence of uncertainties in particle diameter, refractive index and particle shape are analysed.

© 2002 Elsevier Science B.V. All rights reserved.

Keywords: Evanescent wave scattering; Scattering microscopy; Discrete Sources Method

1. Introduction

The wide potential of application of scattering microscopy especially in biology, materials science and information technology gives rise to renewed interest in computer simulation of scattering of evanescent waves by a particle located near a dielectric prism surface [1–3]. In the past mainly scattering by spherical particles has been analysed by approximate models not fully taking into account particle–surface scattering interaction. In recent papers by Doicu et al. [4,5] a computer model for evanescent wave scattering analysis has

been developed based on the Discrete Sources Method (DSM). The model takes into account complete scatterer–prism interaction and provides an opportunity to investigate evanescent wave scattering by any axial symmetric scatterer. It has been demonstrated that only exact models and not just approximate models adequately describe scattering of evanescent waves by a particle near a plane surface [4]. In the present paper we present an improved scheme of DSM enabling to analyse an even larger particle near the plane surface. The new version of DSM gives an extension of its range of validity from particle diameter 1 to 5 μm for an incident wavelength $\lambda_0 = 632.8 \text{ nm}$. The real need to investigate scattering by larger particles consists in the necessity to calibrate modern particle scanner design to be able to demonstrate its ability to measure several orders of magnitude of scattered intensity [3].

* Corresponding author. Tel.: +49-421-218-2507; fax: +49-421-218-5378.

E-mail addresses: eremin@cs.msu.su (Y. Eremin), thw@iwt.uni-bremen.de (T. Wriedt).

2. Discrete Sources Method

In this section a short description of the Discrete Sources Method used for light scattering simulations will be given. Let us start with the statement of the scattering problem. The geometry of the scattering problem is shown in Fig. 1. An axial symmetric particle with a smooth boundary S and interior region D_i is deposited on a plane surface Σ , so that its axis of symmetry coincides with the normal to the plane interface surface. The upper half-space corresponding to the ambient medium is denoted by D_0 , while the lower half-space corresponding to the glass prism is denoted by D_1 . Let us introduce a rectangular coordinate system $Oxyz$ by choosing the origin O at the intersection point between the axis of symmetry and the interface surface. The OZ axis coincides to the symmetry axis and is directed into the domain D_0 . We assume that the incident field $\{\mathbf{E}_1^i, \mathbf{H}_1^i\}$ is a linear polarised plane wave propagating in the glass prism at the angle β_1 with respect to the z -axis. Correspondingly the refracted wave $\{\mathbf{E}_0^i, \mathbf{H}_0^i\}$ is propagating in D_0 at angle θ_0 to the OZ axis, following Snell's law. Then the mathematical statement of the scattering problem can be written as

$$\begin{aligned} \nabla \times \mathbf{H}_t &= ik\varepsilon_t \mathbf{E}_t, & \nabla \times \mathbf{E}_t &= -ik\mu_t \mathbf{H}_t \\ &\text{in } D_t, \quad t = 0, 1, i, \\ \mathbf{n} \times (\mathbf{E}_i - \mathbf{E}_0) &= 0, & \mathbf{n} \times (\mathbf{H}_i - \mathbf{H}_0) &= 0 \\ &\text{on } S, \\ \mathbf{e}_z \times (\mathbf{E}_0 - \mathbf{E}_1) &= 0, & \mathbf{e}_z \times (\mathbf{H}_0 - \mathbf{H}_1) &= 0 \\ &\text{on } \Sigma \end{aligned} \quad (1)$$

and radiation (attenuation) conditions at infinity. Here, \mathbf{n} is the outward unit normal vector to S , $k = \omega/c$ and $\{\mathbf{E}_0, \mathbf{H}_0\}$ stands for the total field in domain D_0 . Note that the total field in D_0 sums the contribution of the refracted incident field and the scattered ones, that is $\mathbf{E}_0 = \mathbf{E}_0^s + \mathbf{E}_0^i$, $\mathbf{H}_0 = \mathbf{H}_0^s + \mathbf{H}_0^i$. If $\text{Im } \varepsilon_t, \mu_t \leq 0$ and the particle surface is smooth enough $S \subset C^{(1,\infty)}$, then the above boundary-value problem is uniquely solvable.

We will construct an approximate solution to the scattering problem via DSM by representing the electromagnetic fields as a finite linear combination of fields of dipoles and multipoles [6,7]. The approximate solution satisfies Maxwell equations in

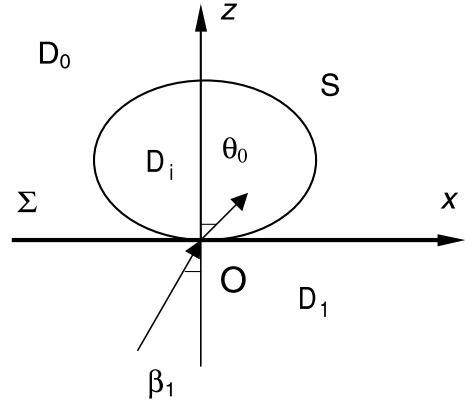


Fig. 1. Geometry of the scattering system.

domains D_t , infinity conditions and the transmission conditions at the plane interface. Essentially, the scattering problem simplifies to the approximation problem of the external excitation on the particle surface. The amplitudes of discrete sources will be determined from the boundary conditions at the particle surface, which can be written as

$$\mathbf{n} \times (\mathbf{E}_i - \mathbf{E}_0^s) = \mathbf{n} \times \mathbf{E}_0^i, \quad \mathbf{n} \times (\mathbf{H}_i - \mathbf{H}_0^s) = \mathbf{n} \times \mathbf{H}_0^i. \quad (2)$$

To fulfil the boundary conditions at the plane interface Σ we consider the Green tensor for a stratified interface [6,7] that is

$$\overset{\leftrightarrow}{\mathbf{G}}(M, M_0) = \begin{bmatrix} \mathbf{g}^{e,h} & 0 & 0 \\ 0 & \mathbf{g}^{e,h} & 0 \\ \frac{\partial f}{\partial x_M} & \frac{\partial f}{\partial y_M} & \mathbf{g}^{h,e} \end{bmatrix}. \quad (3)$$

An approximate solution to the scattering problem will be constructed by taking into account not only the rotational symmetry of the scattering problem geometry but simultaneously the polarisation of the external excitation [6,7]. In this context, for a p-polarised incident field we use the following electric and magnetic vector potentials:

$$\begin{aligned} \mathbf{A}_{mn}^{e,0} &= \{g_m^e(\eta, z_n) \cos(m+1)\phi; \\ &\quad -g_m^e(\eta, z_n) \sin(m+1)\phi; \\ &\quad -f_{m+1}(\eta, z_n) \cos(m+1)\phi\}, \\ \mathbf{A}_{mn}^{h,0} &= \{g_m^h(\eta, z_n) \sin(m+1)\phi; \\ &\quad g_m^h(\eta, z_n) \cos(m+1)\phi; \\ &\quad -f_{m+1}(\eta, z_n) \sin(m+1)\phi\}, \\ \mathbf{A}_{0n}^{e,h,0} &= \{0; 0; g_0^{h,e}(\eta, z_n)\}, \end{aligned} \quad (4)$$

where $g_m^{e,h}$, f_m are Fourier harmonics corresponding Green tensor components, which accept the form

$$g_m^{e,h}(\eta, z_n) = \frac{k_0}{i} Y_m^0(\eta, z_n) + \int_0^\infty J_m(\lambda\rho) v_{11}^{e,h}(z, z_n, \lambda) \lambda^{1+m} d\lambda, \quad (5)$$

$$f_m(\eta, z_n) = \int_0^\infty J_m(\lambda\rho) v_{31}(z, z_n, \lambda) \lambda^{1+m} d\lambda. \quad (6)$$

Here $Y_m^0(\eta, z_n) = h_m^{(2)}(k_0 R_{\eta z_n})(\rho/R_{\eta z_n})^m$, $h_m^{(2)}(\cdot)$ is the spherical Hankel function, (ρ, ϕ, z) are the cylindrical coordinates, $\eta = (\rho, z)$, $R_{\eta z_n}^2 = \rho^2 + (z - z_n)^2$, while $\{z_n\}_{n=1}^\infty$ is a dense set of source points distributed over a segment $\Gamma_z^0 \in D_i$ of the axis of symmetry, and $v_{11}^{e,h}(z, z_n, \lambda)$, $v_{31}(z, z_n, \lambda)$ are corresponding spectral functions which can be found in [4]. They are given by

$$v_{11}^e(\lambda, z, z_n) = \frac{\mu_1 K_0 - \mu_0 K_1}{\mu_1 K_0 + \mu_0 K_1} \frac{1}{K_0} \exp\{-K_0(z + z_n)\}, \quad (7)$$

$$v_{11}^h(\lambda, z, z_n) = \frac{\varepsilon_1 K_0 - \varepsilon_0 K_1}{\varepsilon_1 K_0 + \varepsilon_0 K_1} \frac{1}{K_0} \exp\{-K_0(z + z_n)\}, \quad (8)$$

$z \geq 0, \quad z_n > 0,$

$$v_{31}(\lambda, z, z_n) = \frac{2(\mu_1 \varepsilon_1 - \mu_0 \varepsilon_0)}{(\mu_1 K_0 + \mu_0 K_1)(\varepsilon_1 K_0 + \varepsilon_0 K_1)} \times \exp\{-K_0(z + z_n)\}, \quad (9)$$

where

$$K_t^2 = \lambda^2 - k_t^2, \quad k_t^2 = k^2 \varepsilon_t \mu_t, \quad t = 0, 1. \quad (10)$$

For the total field inside the particle D_i we define the following vector potentials:

$$\mathbf{A}_{mn}^{e,i} = \left\{ J_m^i(\eta, z_n) \cos(m+1)\phi; -J_m^i(\eta, z_n) \sin(m+1)\phi; 0 \right\}, \quad (11)$$

$$\mathbf{A}_{mn}^{h,i} = \left\{ J_m^i(\eta, z_n) \sin(m+1)\phi; J_m^i(\eta, z_n) \cos(m+1)\phi; 0 \right\}, \quad (12)$$

$$\mathbf{A}_{0n}^{e,h,i} = \left\{ 0; 0; J_0^i(\eta, z_n) \right\}, \quad (13)$$

where $J_m^i(\eta, z_n) = j_m(k_i R_{\eta z_n})(\rho/R_{\eta z_n})^m$, $\{z_n\}_{n=1}^\infty$ be a dense set of points distributed over a segment $\Gamma_z^i \in D_i$ of the axis of symmetry and $j_m(\cdot)$ are spherical Bessel functions. Let us introduce the following notations:

$$\begin{aligned} \overleftrightarrow{\mathbf{R}}_1^t &= \begin{pmatrix} i/k\varepsilon_t \mu_t \nabla \times \nabla \times \\ -1/\mu_t \nabla \times \end{pmatrix}, \\ \overleftrightarrow{\mathbf{R}}_2^t &= \begin{pmatrix} 1/\varepsilon_t \nabla \times \\ i/k\varepsilon_t \mu_t \nabla \times \nabla \times \end{pmatrix}. \end{aligned} \quad (14)$$

Now we can represent the approximate solution of the scattering problem for a p-polarised field as

$$\begin{aligned} \begin{pmatrix} \mathbf{E}_t^N \\ \mathbf{H}_t^N \end{pmatrix} &= \sum_{m=0}^M \sum_{n=1}^{N_t^m} \left\{ P_{mn}^t \overleftrightarrow{\mathbf{R}}_1^t \mathbf{A}_{mn}^{e,t} + q_{mn}^t \overleftrightarrow{\mathbf{R}}_2^t \mathbf{A}_{mn}^{h,t} \right\} \\ &+ \sum_{n=1}^{N_t^0} P_n^t \overleftrightarrow{\mathbf{R}}_1^t \mathbf{A}_{0n}^{e,t}, \quad t = 0, i. \end{aligned} \quad (15)$$

The last term in (15) is associated to the vertical electric dipoles. Here, N is a complex index incorporating M and N_t^M .

The main differences of the current approach from the conventional DSM scheme [6,7] consist in the following:

1. Different numbers of discrete sources (DS) are possible for the representation of the scattered field in D_0 and total field inside the particle D_i . The numbers of discrete source are chosen proportionally to the ratio of refractive indexes of the corresponding media. For the internal domain (higher refractive index) we use a larger number of discrete sources then for scattered field, because our primary goal is to approximate the external excitation (the transmitted plane wave in D_0) on a particle surface. Although such representations have been published before [6] they have not yet been realised in a computational model.

2. The number of discrete sources now depends on the rank of the Fourier harmonic $N_t^m = N_t(m)$. For a higher rank of the harmonic we use a lower number of discrete sources. This situation seems to be similar to the T-matrix approach or any other method using spherical vector wave functions. In this case the higher the rank of the azimuth harmonic, the less number of spherical functions are

need for approximation. From computer simulation analysis for large particles we found that the surface residual for the higher harmonics increases if we retain the same number of discrete sources for all Fourier harmonics. This circumstance enables to acquire a more accurate simulation result, provide a monotone decrease of the surface residual and to reduce the demand on computer resources up to 30% for a larger sphere compared to the conventional DSM model.

3. For large particles higher Fourier harmonics are computed using advanced Fresnel approximation for Weyl integrals [8].

As before we employ a convergence test and a posterior surface residual estimate (in mean square sense) to validate the results obtained. This explicatively means that a monotone decrease (with increasing numbers of M and N) of the surface residual and the scattered field stability ensures that we reach a correct simulation result. At the same time we would like to remind that we have already made a series of comparisons of the conventional DSM model with a T-matrix programme [4].

All these innovations allow an increased accuracy of the numerical results (that is a diminished surface residual by several orders), reduced computer time and extending the range of validity of the DSM from particle diameter of 1 up to 5 μm . The completeness of the system of distributed multipoles being used in (15) guarantees the convergence of the approximate solution to the exact solution in a closed subset of D_0 [9].

As mentioned before the above representations satisfy all the conditions of the scattering problem except the transmission condition at the particle surface (2). In fact this condition will be used to determine the amplitudes of discrete sources $\{P_{mn}^i, q_{mn}^i, r_n^i\}$. Various numerical schemes for amplitude determination are at our disposal. It has been found that more stable results can be obtained by using a generalised collocation technique and pseudo-inversion of an over-determined system of linear equations. A posterior surface residual evaluation makes it possible to control the error of the result obtained.

After the amplitudes of the discrete sources have been determined, one can calculate the far-

field pattern (scattering diagram) $\mathbf{E}_\infty^0(\theta, \phi)$, which is determined in the upper part of the unit sphere $\Omega = \{0^\circ \leq \theta < 90^\circ, 0^\circ \leq \phi \leq 360^\circ\}$ and is given by

$$\mathbf{E}_\infty^s(M)/|\mathbf{E}^0(z=0)| = \frac{\exp\{-ik_0R\}}{R} \mathbf{E}_\infty^0(\theta, \phi) + O(R^{-2}),$$

$$R = |M| \rightarrow \infty, \quad z > 0. \quad (16)$$

We use an asymptotic approach for the Weyl–Sommerfeld integrals [7], which leads to the following representation for the θ, ϕ -components of the scattering diagram corresponding to the representation (15)

$$E_{\infty, \theta}^0(\theta, \phi) = ik_0/\varepsilon_0 \sum_{m=0}^M \cos(m+1)\phi \phi(ik_0/\varepsilon_0 \sin \theta)^m$$

$$\times \sum_{n=1}^{N_0^m} \left\{ P_{nm}^0 \cos \theta \left[\gamma'_n + (v^e - v \sin^2 \theta) \gamma_n \right] \right.$$

$$\left. + q_{nm}^0 (\gamma'_n + v^h \gamma_n) \right\} - ik_0/\varepsilon_0 \sin \theta$$

$$\times \sum_{n=1}^{N_0^0} r_n^0 (\gamma'_n + v^h \gamma_n), \quad (17)$$

$$E_{\infty, \phi}^0(\theta, \phi) = -ik_0/\varepsilon_0 \sum_{m=0}^M \sin(m+1)\phi \phi(ik_0/\varepsilon_0 \sin \theta)^m$$

$$\times \sum_{n=1}^{N_0^m} \left\{ P_{nm}^0 (\gamma'_n + v^e \gamma_n) + q_{nm}^0 \right.$$

$$\left. \times \cos \theta \left[\gamma'_n + (v^h - v \sin^2 \theta) \gamma_n \right] \right\}, \quad (18)$$

where the associated spectral functions accept the form

$$v^e = \frac{i \cos \theta - \kappa}{i \cos \theta + \kappa}, \quad v^h = \frac{i \varepsilon_1 \cos \theta - \varepsilon_0 \kappa}{i \varepsilon_1 \cos \theta + \varepsilon_0 \kappa},$$

$$v = \frac{2(\varepsilon_1 - \varepsilon_0)}{(i \cos \theta + \kappa)(i \varepsilon_1 \cos \theta + \varepsilon_0 \kappa)}, \quad (19)$$

$$\kappa = \sqrt{\sin^2 \theta - \varepsilon_1/\varepsilon_0},$$

$$\gamma_n = \exp\{-ik_0 z_n \cos \theta\},$$

$$\gamma'_n = \exp\{ik_0 z_n \cos \theta\}. \quad (20)$$

So, the scattering diagram (17) and (18) is represented as a finite linear combination of elementary functions once the unknown amplitudes of discrete sources are determined. This circumstance allows

an economic computer analysis of the scattering characteristics in the wave zone.

3. Results and discussion

In this section we will numerically analyse scattering of an evanescent wave by a particle deposited on a glass prism. The wavelength of the external excitation in free space is assumed to be $\lambda_0 = 632.8$ nm. The scatterer is deposited on a glass prism with a refractive index of $n_1 = 1.52$ [3]. So, the evanescent wave appears for incident angles $\beta_1 > \beta_c$ where $\beta_c = \arcsin(n_0/n_1)$ [4], for our case $\beta_c \approx 41.14^\circ$. We will analyse the Differential Scattering Cross-section (DSC) in the plane of incidence for a p-polarised plane wave excitation, which is given by

$$\text{DSC}(\theta, \phi) = |E_{\infty, \theta}^0(\theta, \phi)|^2 + |E_{\infty, \phi}^0(\theta, \phi)|^2. \quad (21)$$

Here $E_{\infty, \theta, \phi}^0(\theta, \phi)$ are the components of the scattering diagram (17) and (18). In Fig. 2 we plot the DSC (21) in the incident plane for polystyrene latex (PSL) sphere ($n_i = 1.6$) with a diameter $3.0 \mu\text{m}$ [3] and three incident angles. Two of them $\beta_1 = 41.7^\circ, 48.3^\circ$ belong the region of evanescent waves. One of the most interesting features of the results is degradation of the DSC maximum in the forward direction. Similar results have been obtained in [3] (see Figs. 2, 4, 6) by using direct measurements of DSC. In our case M was chosen as $M = 16$ (this is our sense equivalent to retaining 35 Fourier harmonics). We did a convergence test and found that M values 16, 18, 20 give the same scattered intensity (in the frame of two digits) both in the ZX and the ZY planes. For this case the DS numbers were $N_i^0 = 51, N_e^0 = 37; N_i^{14} = 28, N_e^{14} = 21$. For the conventional DSM model we set ($N_i = 51, N_e = 37$, they are independent on harmonic's number) and we acquired very close values of the scattered intensity except at its minimal values. Besides, in the last case the surface residual was three times higher then obtained with the new DSM model. Total time of calculation on Pentium III-850 was 40 s. One can see that small changes in the incident angle cause essential changes in the shape and amplitude of the DSC. With the last incident angle the forward scattering peak seen at

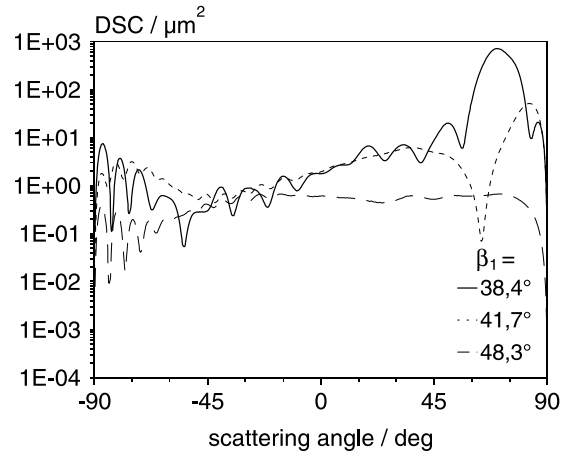


Fig. 2. Differential Scattering Cross-section (DSC in μm^2 units) in the incident plane versus scattering angle θ for PSL spherical particle with diameter of $d = 3 \mu\text{m}$ and refractive index of $n_i = 1.6$. p-Polarised plane wave strikes the sphere from glass, refractive index $n_1 = 1.52$. Three incident angles $\beta_1 = 38.4^\circ, 41.7^\circ$ and 48.3° are considered. The wavelength of excitation is 632.8 nm.

the other incident angle vanishes. DSC corresponding to a sphere diameter variation of 10% is depicted in Fig. 3 for an incident angle of $\beta_1 = 41.7^\circ$. It is clear that 10% of diameter variation leads to the visible changes of DSC. Besides variation in diameter there might be some variation of refractive index. DSC associated with refractive index variation – 1.25% ($n_i = 1.58$) is shown at Fig. 4. Also in this case there are apparent differences between the different DSCs. Fig. 5 demonstrates the influence of sphere deformations on a DSC diagram. We use prolate (aspect ratio=1.05) and oblate spheroids which are equivolume to the sphere of diameter $d = 3 \mu\text{m}$. Even with this low aspect ratio there are large differences compared to the corresponding sphere-scattering diagram apart from the forward scattering peak. Finally in Fig. 6 we demonstrate the results associated with DSC scattered by the original sphere ($d = 3 \mu\text{m}, n_i = 1.6$) and an distorted particle which is an oblate spheroid with an equivolume diameter $d = 2.7 \mu\text{m}, n_i = 1.58$, aspect ratio=1.05. In the last case the total number of harmonics is (with $M = 15$) $N_i^0 = 35, N_e^0 = 26; N_i^{13} = 23, N_e^{13} = 18$ and the total time of

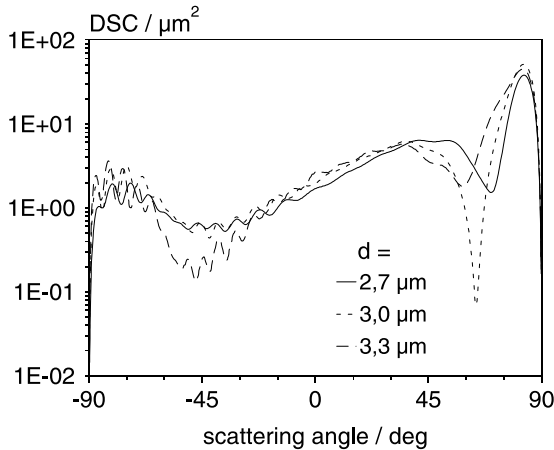


Fig. 3. DSC in the incident plane corresponds to PSL spheres of three different diameters $d = 2.7, 3$ and $3.3 \mu\text{m}$. The incident angle is $\beta_1 = 41.7^\circ$, p-polarisation.

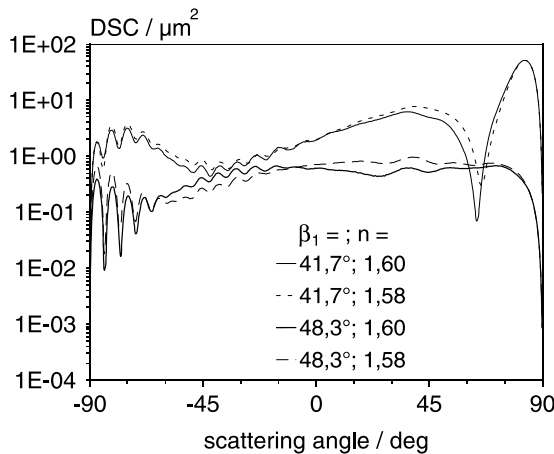


Fig. 4. DSC for PSL sphere $d = 3 \mu\text{m}$ and incidences are $\beta_1 = 41.7^\circ$ and 48.3° . Influence of a variation of refractive index $n_i = 1.6$ and $n_i = 1.58$ is considered.

calculation is 25 s on Pentium III-850. It is clear that uncertainties in the particle diameter, refractive index or particle deformation can cause a problem for modern particle scanner design calibration. Thus an advanced light scattering model like the proposed method would be needed to take into account the various effect of particle–surface interaction, particle non-sphericity and refractive index uncertainties.

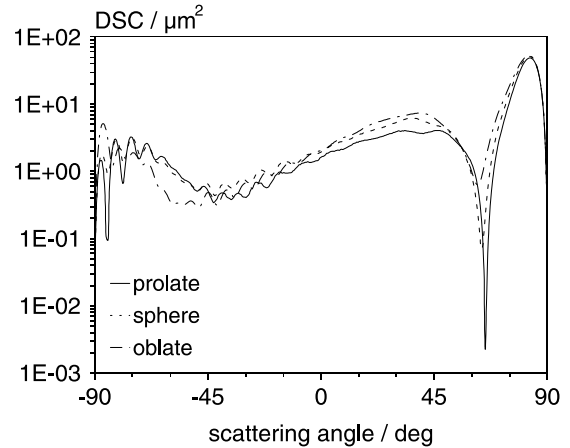


Fig. 5. DSC for PSL particle equivalent volume $d = 3 \mu\text{m}$ and incidence $\beta_1 = 41.7^\circ$. Particle deformation in the frame of spheroidal shape (aspect ratio = 1.05) prolate–sphere–oblate is examined.

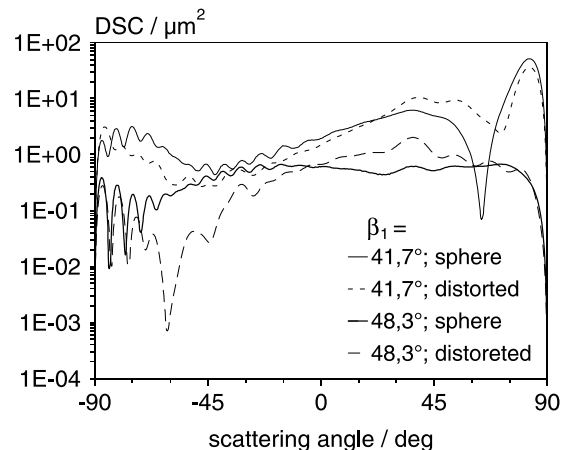


Fig. 6. DSC for PSL sphere $d = 3 \mu\text{m}$ ($n_i = 1.6$) and distorted particle (equivalent volume oblate spheroid aspect ratio = 1.05, $n_i = 1.58$) are considered. Incident angles are $\beta_1 = 41.7^\circ$ and $\beta_1 = 48.3^\circ$.

4. Conclusions

An extended version of DSM, which enables to analyse evanescent wave scattering by a large non-spherical particle, has been presented. Computer simulation results have shown that uncertainties in particle diameter, refractive index and shape can cause a problem for particle scanner design

calibration especially in the field of evanescent wave scattering.

Acknowledgements

We gratefully acknowledge funding of this research by Deutsche Forschungsgemeinschaft (DFG).

References

- [1] Ch. Girard, A. Dereux, *Rep. Prog. Phys.* 59 (1996) 657.
- [2] M. Quinten, A. Pack, R. Wannemacher, *Appl. Phys. B* 68 (1999) 87.
- [3] M.J. Jory, S.N. Swatton, E. Perkins, N.J. Geddes, J.R. Sambles, *J. Modern Opt.* 48 (2001) 565.
- [4] A. Doicu, Yu.A. Eremin, T. Wriedt, *Comput. Phys. Commun.* 134 (2001) 1.
- [5] A. Doicu, Yu.A. Eremin, T. Wriedt, *Opt. Commun.* 190 (2001) 5.
- [6] Y.A. Eremin, N.V. Orlov, A.G. Sveshnikov, in: T. Wriedt (Ed.), *Generalized Multipole Techniques for Electromagnetic and Light Scattering*, Elsevier Science, Amsterdam, 1999, p. 39.
- [7] Yu. Eremin, N. Orlov, *Appl. Opt.* 35 (1996) 6599.
- [8] V.I. Ivakhnenko, J.C. Stover, Yu. Eremin, in: Th. Wriedt, Yu. Eremin (Eds.), *Electromagnetic and Light Scattering – Theory and Applications III*, Universität Bremen, Bremen, 1998, p. 125.
- [9] A. Doicu, Yu. Eremin, T. Wriedt, *Acoustic and Electromagnetic Scattering Analysis Using Discrete Sources*, Academic Press, London, 2000.